

# Supplementary Information

## Direct Observation of the Ultrafast Exciton Dissociation in Lead-iodide Perovskite by 2D Electronic Spectroscopy

Ajay Jha<sup>1</sup>, Hong-Guang Duan<sup>1,2,3</sup>, Vandana Tiwari<sup>1,4</sup>, Pabitra Nayak<sup>5</sup>,  
Henry J. Snaith<sup>5</sup>, Michael Thorwart<sup>2,3</sup>, and R. J. Dwayne Miller<sup>1,3,6</sup>

<sup>1</sup>*Max Planck Institute for the Structure and Dynamics of Matter,  
Luruper Chaussee 149, 22761 Hamburg, Germany*

<sup>2</sup>*I. Institut für Theoretische Physik, Universität Hamburg, Jungiusstraße 9, 20355 Hamburg, Germany*

<sup>3</sup>*The Hamburg Center for Ultrafast Imaging, Luruper Chaussee 149, 22761 Hamburg, Germany*

<sup>4</sup>*Department of Chemistry, University of Hamburg,  
Martin-Luther-King Platz 6, 20146 Hamburg, Germany*

<sup>5</sup>*Department of Physics, University of Oxford, Clarendon Laboratory,  
Parks Road, Oxford OX1 3PU, United Kingdom*

<sup>6</sup>*The Departments of Chemistry and Physics, University of Toronto,  
80 St. George Street, Toronto Canada M5S 3H6*

(Dated: November 16, 2017)

In this Supplementary Information, we provide more details on the scanning electron micrograph (SEM) data, on calculating the photo-generated carrier and exciton density, on the FROG trace, the global fitting approach and the two-dimensional (2D) correlation analysis. In addition to the room-temperature measurement, we also measured the 2D electronic spectra at 180 K, which are presented here. The time scale of the electronic dephasing of the exciton and free carriers are estimated by the anti-diagonal bandwidth of the corresponding spectrum. Moreover, we show the 2D vibrational map revealed in the experiment.

### I. SCANNING ELECTRON MICROGRAPH

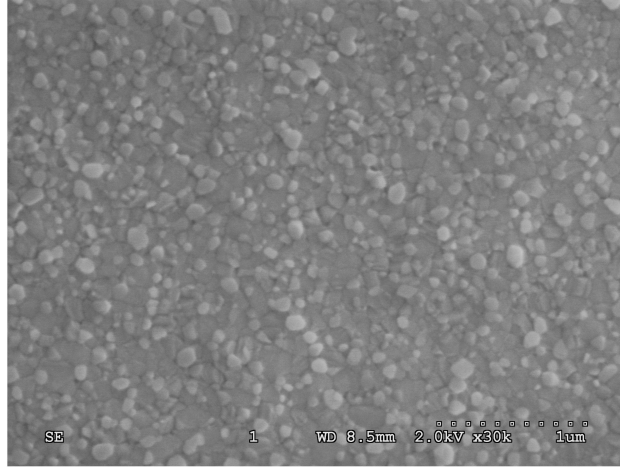


FIG. S1. Scanning Electron Micrograph of the MAPbI<sub>3</sub> thin film.

### II. PHOTOGENERATED EXCITON AND CARRIER DENSITIES

In this section, we calculate the exciton and free-carrier densities. The exciton Bohr radius is given by

$$a = a_0 \epsilon_r \frac{m_e}{\mu}, \quad (\text{S1})$$

where  $a_0 = 0.53\text{\AA}$ , the dielectric constant  $\epsilon_r = 6.5$  [1] and reduced mass  $\mu = 0.104m_e$  [2]. Thus, the calculated exciton radius is  $a = 33\text{\AA}$ . With the exciton radius, we calculate the Mott density. The exciton scattering occurs when the

exciton wavefunctions overlap, which happens when the exciton-exciton distance is equal to the exciton diameter. The density at this situation is called the Mott density. It is given approximately by the inverse volume of the exciton, i.e.,  $N_{Mott} = \frac{1}{\frac{4\pi a^3}{3}} = 2 \times 10^{19} \text{cm}^{-3}$ .

Secondly, we have calculated the photogenerated exciton density for our experimental setup. The exciton density is calculated by  $n_0 = j\alpha$ , where  $j$  is the pump fluence (photons  $\text{cm}^{-2}$ ) and  $\alpha$  is the absorption coefficient at pump  $\lambda$ . 2D spectroscopic measurements have been performed at three different energies: 5, 10 and 18 nJ with the beam diameter 100  $\mu\text{m}$  at the focal point. Even for the largest beam energy of 18 nJ ( $\sim 7 \times 10^{14}$  photons  $\text{cm}^{-2}$ ),  $n_0 = 7 \times 10^{18}$  is three times less than the Mott density.

Similarly, we have calculated the photo-generated carrier density. Using the value of the absorption coefficient of  $2 \times 10^4 \text{cm}^{-1}$  at  $13500 \text{cm}^{-1}$ , the carrier density is estimated to be  $\sim 1.4 \times 10^{19}$  for the excitation pulse energy of 18 nJ. For the experiments performed at 5 and 10 nJ, the carrier density has been estimated to be  $4 \times 10^{18}$  and  $8 \times 10^{18}$ , respectively.

### III. CHIRP DETECTION

In our measurements, the main observation is ultrafast dissociation of free excitons with the time scale of 50 fs. Moreover, we also observe short-lived electronic coherence which lives within the electronic dephasing time scales. For such short time scale, it is necessary to examine the artifacts generated on the substrate without the sample. This can, for instance, be done by characterizing the pulse chirp and measure the photon-echo (PE) signal generated by the substrate at the pulse overlapped region. In Fig. S2, we show the measured transient grating FROG trace of the substrate at the sample position in the cryostat without the sample. We observe that the generated PE signal shows  $\sim 5$  counts at  $T = 0$  fs and completely decays to zero within 20 fs. For comparison, we observe the corresponding PE signal in the presence of the sample with  $\sim 70$  counts. Thus, in the measurement, only  $\sim 7\%$  of the total PE signal stems from the substrate at  $T=0$  fs. Based on the observation of the profile of the FROG trace, we do not observe any evidence of the linear and high-order chirp. This finding demonstrates that the observed ultrafast dynamics is generated from perovskites and is not an artifact from the substrate.

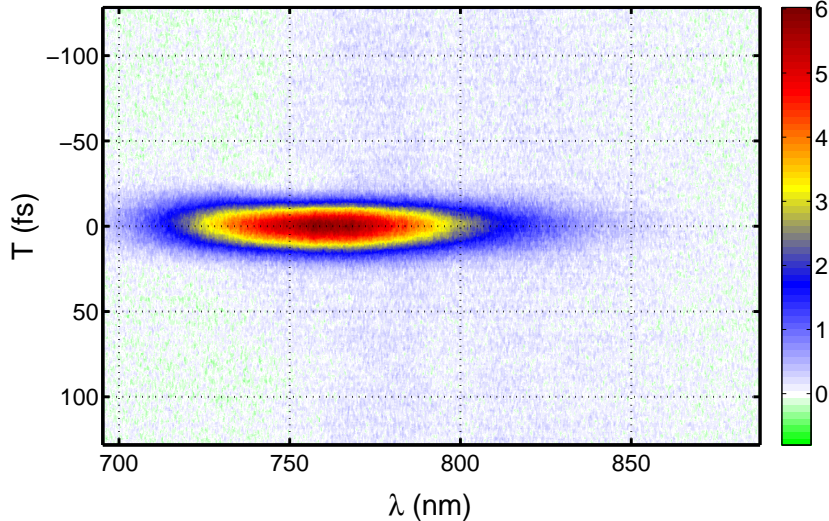


FIG. S2. Transient grating FROG trace from the quartz substrate (2 mm thickness) in absence of the sample. It shows the PE signal with a maximum magnitude of 5 counts at  $T=0$  fs which completely decays to zero within 20 fs. Based on the measured FROG-trace profile, we can conclude that there is no linear or high-order chirp generated.

### IV. TIME-DEPENDENT DIAGONAL BANDWIDTH IN THE 2D SPECTRA

In Fig. S3, we show the time-evolved diagonal bandwidth of the 2D electronic spectra at room temperature. It shows that the central peak is dramatically shrunk along the diagonal cut within the initial 500 fs.

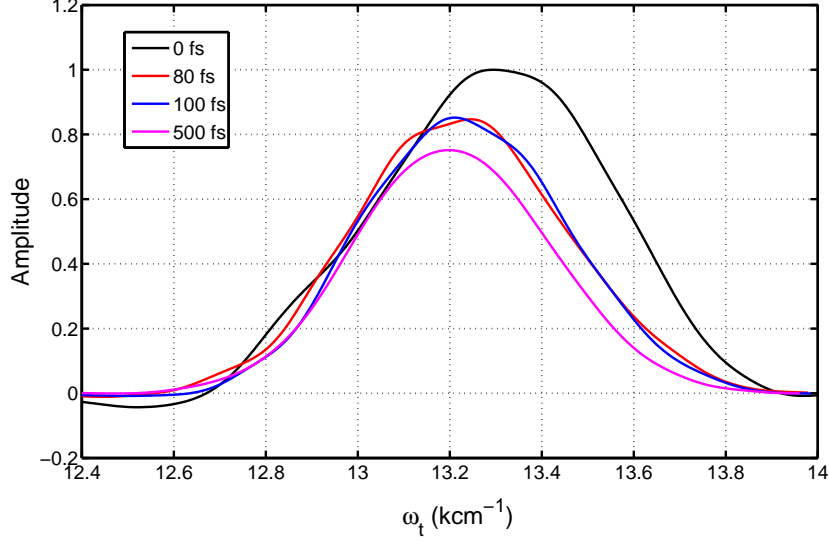


FIG. S3. The time-evolved diagonal bandwidth along the 2D spectra at room temperature. It is clearly visible that the exciton and free-carrier peaks are significantly shrunk within the initial 500 fs.

## V. GLOBAL FITTING APPROACH

Multidimensional global fits of both experimental and measured arrays of 2D spectra were performed in accordance with the previously developed algorithm [3]. A detailed description can be found in the SI of Ref. [4]. In this method, a sequence of 2D spectra taken at different  $T$  values is collected to form a three-dimensional array  $S(\omega_\tau, \omega_t, T)$ . This 3D array is then decomposed into a sum of two-dimensional decay-associated spectra  $A_i(\omega_t, \omega_\tau)$  with individual exponential decays with correspondingly associated lifetimes  $\tau_i$  according to

$$S(\omega_\tau, \omega_t, T) = \sum_i A_i(\omega_\tau, \omega_t) \exp(-T/\tau_i). \quad (\text{S2})$$

## VI. TWO-DIMENSIONAL CORRELATION MAP

To verify the origin of the oscillations observed in the 2D electronic spectra, we performed a cross-correlation analysis of the residuals across  $\omega_\tau = \omega_t$  [3]. The residual  $R(\omega_t, \omega_\tau, T)$  is obtained by subtracting the globally fitted kinetics from the real part of the total 2D electronic spectra. Then, we calculate the correlation coefficients  $C$  between two residuals of a pair of conjugated spectral positions in the delay time window up to 2 ps. The delay time steps are equally distributed with intervals of 10 fs. The correlation coefficients are defined as

$$C(\omega_t, \omega_\tau) = \text{corr}[R(\omega_t, \omega_\tau, T), R(\omega_\tau, \omega_t, T)], \quad (\text{S3})$$

where the correlation is evaluated with the respect to  $T$ .

In Fig. S4, we plot the 2D correlation map of the residuals obtained after the global fitting of the time sequence of 2D spectra. It shows one cross peak at  $(\omega_t, \omega_\tau) = (12700, 13600) \text{ cm}^{-1}$  with small positive magnitude. Moreover, several negative peaks can be clearly resolved at the free-carrier band ( $> 13500 \text{ cm}^{-1}$ ). Based on Ref. [5], the correlation (positive peak) indicates the electronic coherence and the anti-correlation (negative peak) manifests the vibrational coherence. Thus, the strong negative peaks at the free-carrier band shows strong evidence of vibrational coherence. To identify the cross peaks, we marked it by the dashed lines at  $13600 \text{ cm}^{-1}$ ,  $13820 \text{ cm}^{-1}$  and  $14020 \text{ cm}^{-1}$ . They indicate the resolved vibrations with a frequency of  $220 \text{ cm}^{-1}$ . It coincides with the vibration of  $196 \text{ cm}^{-1}$  retrieved from the power spectrum in the main text (Fig. 4). Moreover, the weak positive peak at  $(12700, 13600) \text{ cm}^{-1}$  provides evidence of the electronic coherence in that frequency region, which is close to the energy gap between the exciton and the free-carrier band (the mismatch is due to the off-centered peaks in the 2D spectra). Based on this correlation analysis,

we have evidence of the electronic coherence between exciton and the free carriers and the vibrational coherence in the free-carrier band.

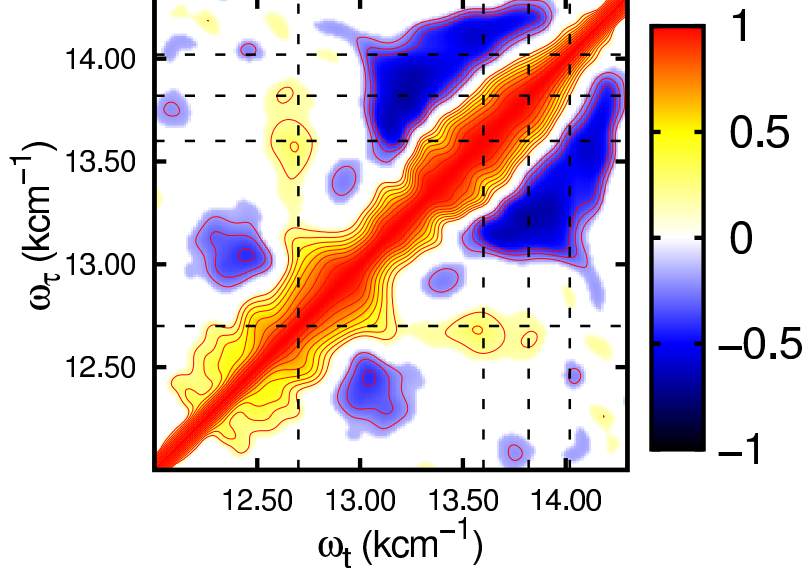


FIG. S4. Correlation 2D spectrum of residuals obtained after the 3D global fitting of the 2D spectra. Positive magnitude indicates correlation while negative manifests anticorrelation.

## VII. 2D ELECTRONIC SPECTRUM AND ITS DEPHASING AT LOW TEMPERATURE

In addition to the room-temperature measurement reported in the main paper, we have also measured the 2D electronic spectra of perovskite at 180 K. The measured data are shown in Fig. S5. In Fig. S5(a), two diagonal peaks are clearly visible at  $\omega_\tau = 13100 \text{ cm}^{-1}$  and  $13600 \text{ cm}^{-1}$ , respectively. These two peaks allow us to obtain the exciton binding energy ( $\sim 12 \text{ meV}$ ) at 180 K, which is not significantly changed compared to the one measured at room temperature. The associated time scales of the electronic dephasing can be extracted from the linewidth of their profiles along the anti-diagonals of the peaks shown in Figs. S5(b) and S5(c). Based on the fitting of the anti-diagonal peak with a Lorentzian lineshape function, the obtained timescales of the electronic dephasing are 49 fs and 51 fs, respectively.

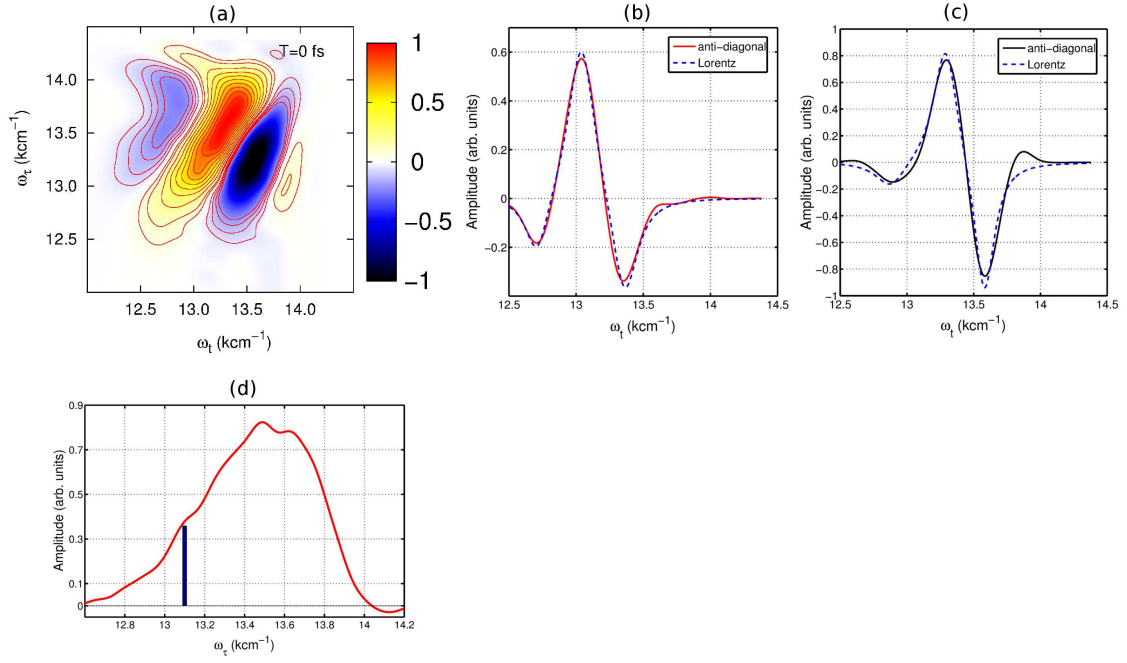


FIG. S5. (a) Real part of the measured 2D electronic spectrum at  $T = 0$  fs at 180 K. The anti-diagonal profiles of the exciton and the free-carrier transitions are marked by the red and black dashed lines, respectively. The extracted profiles of the exciton (red curve) and the free carrier (black curve) transitions are shown in (b) and (c), respectively. The associated linewidth is estimated by the fit to a Lorentzian lineshape function. This yields the line widths of  $253$  and  $228$   $\text{cm}^{-1}$ , which gives the time scales of the electronic dephasing of  $41 \pm 1.5$  fs and  $45 \pm 1.5$  fs, respectively. (d), The diagonal cut of the 2D electronic spectrum at  $T=0$  fs. The exciton peak is more clear to be resolved at 180 K.

## VIII. FOURIER TRANSFORM OF PEAK D IN THE 2D SPECTRUM

In Fig. S6, we show the Fourier spectrum associated with the oscillatory dynamics of the peak D in Fig. 2 of the main text. It is obtained by Fourier transforming the residual after subtracting the global kinetics by the global fitting approach.

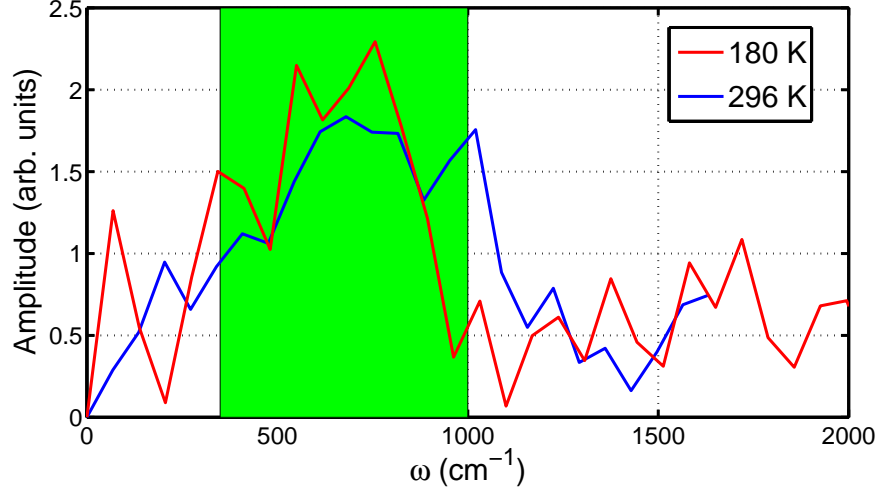


FIG. S6. Fourier spectrum of the time evolution signal of peak D after removing the kinetics by the global fitting approach. One broadband peak centered at  $750 \text{ cm}^{-1}$  indicates a short lifetime of the oscillations. We observe that the Fourier spectrum measured at different temperatures (296K and 180 K) are very similar within our experimental resolution.

## IX. 2D VIBRATIONAL MAP

In Fig. S7, we show the maps of the vibrational modes detected from the measurements. After fitting the residuals to the experimental data, we have applied a numerical Fourier transform to the real parts. This provides a 3D spectrum of residuals along the dimensions  $\omega_t$ ,  $\omega_\tau$  and  $\omega_T$ . The frequency range is limited to  $1667 \text{ cm}^{-1}$  and the frequency resolution is  $\sim 16 \text{ cm}^{-1}$  since the maximum waiting-time window was up to 2 ps with the time step of 10 fs. In the 2D vibrational maps, the vibrational mode with frequency of  $176 \text{ cm}^{-1}$  and  $192 \text{ cm}^{-1}$  shows the largest magnitude. This finding coincides with the observation obtained from the power spectrum (Fig. 4(d)) in the main text. In addition, the other two low-frequency modes are resolved, with frequencies of  $48 \text{ cm}^{-1}$  and  $96 \text{ cm}^{-1}$ . Moreover, high-frequency modes ( $673, 770, 833, 1075, 1203, 1267, 1508, 1572$  and  $1620 \text{ cm}^{-1}$ ) are clearly identified from the 2D vibrational analysis with smaller magnitude.

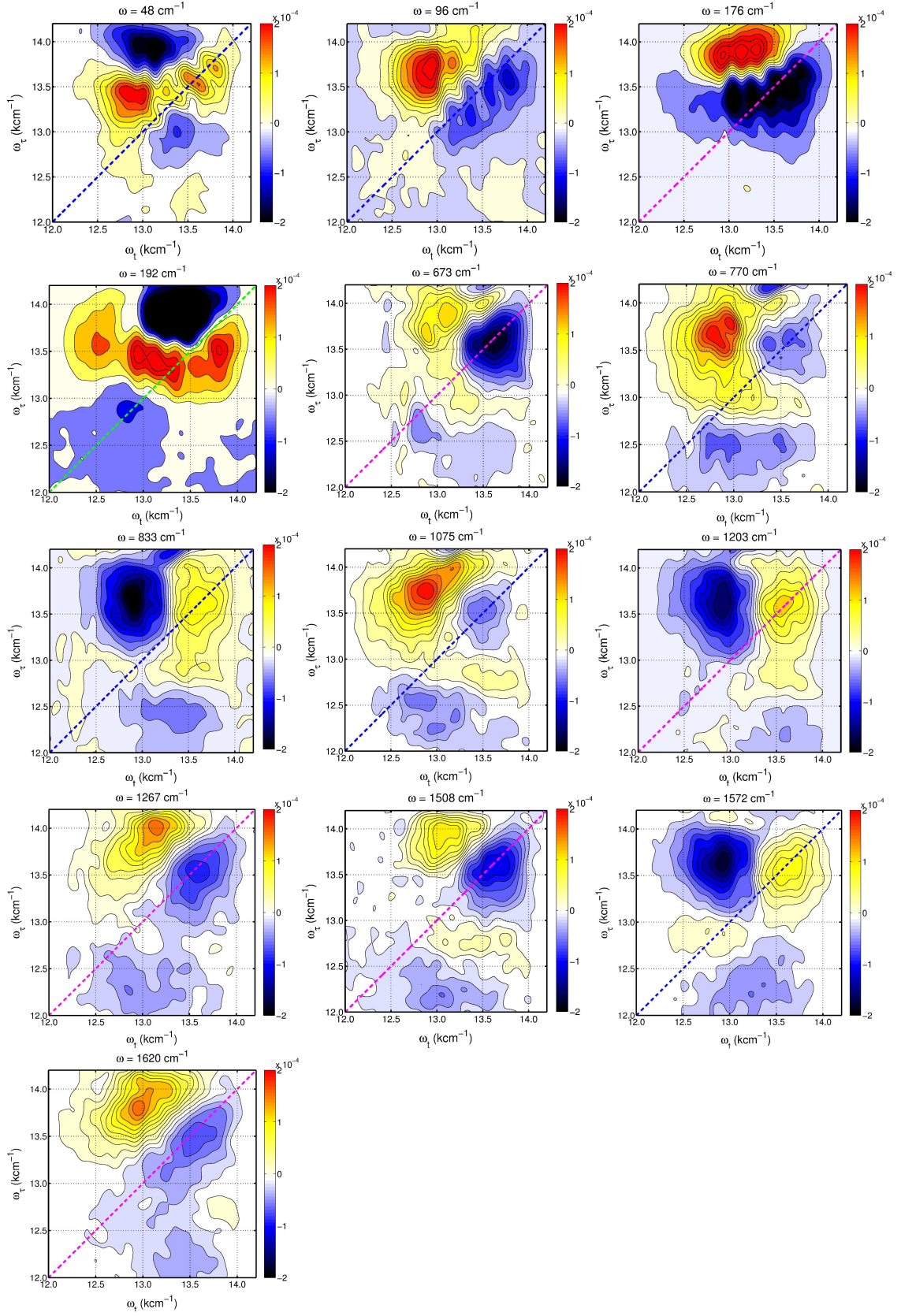


FIG. S7. Frequency-resolved 2D vibrational maps from residuals after removing the kinetics by the global fitting approach. In the measurement, we detect the 2D spectra up to 2 ps with the equally distributed time step of 10 fs, which give us the detection window of  $1660 \text{ cm}^{-1}$  with the frequency resolution of  $\sim 16$  fs.

- 
- [1] Tanaka, K.; Takahashi, T.; Ban, T.; Kondo, T.; Uchida, K.; Miura, N. *Solid State Comm.* **2003**, *127*, 619-623.
- [2] Miyata, A.; Mitioglu, A.; Plochocka, P.; Portugall, O.; Wang, J. T.; Stranks, S. D; Snaith H. J.; Nicholas, R. J. *Nat. Phys.* **2015**, *11* 582-587.
- [3] Prokhorenko, V. I. *European Photochemistry Association Newsletter*; June 2012, p 21.
- [4] Milota, F.; Prokhorenko, V. I.; Mancal, T.; Berlepsch, H. von; Bixner, O.; Kauffmann, H. F.; Hauer, J. *J. Phys. Chem. A* **2013**, *117* 6007-6014.
- [5] Butkus, V.; Zigmantas, D.; Valkunas, L.; Abramavicius, D. *Chem. Phys. Lett.* **2012**, *545* 40-43.